Article

Anticancer, Antioxidant, and Catalytic Activities of Green Synthesized Gold Nanoparticles Using Avocado Seed Aqueous Extract

Yonela Ngungeni, Jumoke A. Aboyewa, Koena L. Moabelo, Nicole R. S. Sibuyi, Samantha Meyer, Martin O. Onani, Mervin Meyer, and Abram M. Madiehe*

Read Online

| ACCESS | Metrics & More | Article Recommendations | Supporting Information |

ABSTRACT: Disposal of agricultural waste has a negative impact on the environment and human health and may contribute to the greenhouse effect. The field of nanotechnology could provide alternative solutions to upcycle agricultural wastes in a safer manner into high-end value products. Organic waste from plants contain biomaterials that could serve as reducing and capping agents in the synthesis of nanomaterials with enhanced activities for use in biomedical and environmental applications. *Persea americana* (avocado) is a fruit with a high nutritional value; however, despite its rich phytochemical profile, its seed is often discarded as waste. Therefore, this study aimed to upcycle avocado seeds through the synthesis of gold nanoparticles (AuNPs) and evaluate their anticancer, antioxidant, and catalytic activities. The biosynthesis of avocado seed extract (AvoSE)-mediated AuNPs (AvoSE−AuNPs) was achieved following the optimization of various reaction parameters, including pH, temperature, extract, and gold salt concentrations. The AvoSE−AuNPs were poly-dispersed and anisotropic, with average core and hydrodynamic sizes of 14 ± 3.7 and 101.39 ± 1.4 nm, respectively. The AvoSE−AuNPs showed excellent antioxidant potential in terms of ferric reducing antioxidant power (343.88 ± 0.001 μmolAAE/L), 2,2-diphenyl-1-picrylhydrazyl (128.80 ± 0.0159 μmolTE/L), and oxygen radical absorbance capacity (1822.02 ± 12.6338 μmolTE/L); significantly reduced the viability of Caco-2 and PC-3 cells in a dose-dependent manner; and efficiently reduced 4-nitrophenol (4-NP) to 4-aminophenol. This study demonstrated how avocado seeds, an agricultural waste, can be used as sources of new bioactive materials for the synthesis of AuNPs, which have excellent antioxidant, anticancer, and catalytic activities, showing AvoSE−AuNPs' versatility in various applications. In addition, the AvoSE−AuNPs exhibited good stability and recyclability during the catalytic activity, which is significant because some of the primary issues with the use of metallic NPs as catalysts are around the cost-effectiveness, recovery, and reusability of the catalyst.
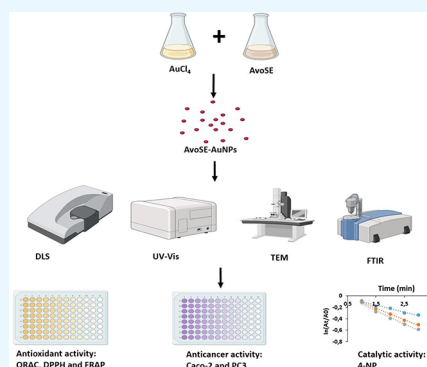
1. INTRODUCTION

Gold nanoparticles (AuNPs) are one of the most widely studied nanoparticles (NPs) due to their unique physiochemical properties and good chemical stability, which can be leveraged in a broad range of applications including catalysis, bio-labeling, diagnostics, and drug delivery.[1−4] Chemical and physical reduction methods are no doubt the most common and widely used methods for AuNP preparation. However, these methods utilize toxic chemicals and physical processes which are expensive, require high-energy consumption, and subsequently produce nanoproducts that can be harmful.[5−8] Consequently, their use in clinical and biomedical applications is constrained despite the considerable potential of NPs.[6,8] Therefore, there is a need for the development of green synthesis methods which are more environmentally friendly and can produce NPs that are more reliable and biologically compatible.

Green nanotechnology is a maturing field of nanotechnology that serves as an alternative to chemical and physical methods for the synthesis of NPs.[9] The green synthesis approach uses natural products from bacteria, fungi, enzymes, plants, and biopolymers for the production of NPs.[10−14] Green synthesis of NPs using plants or plant products is an approach that interconnects nanotechnology and plant biotechnology.[15] Using plants for the synthesis NPs provides a reliable and simple approach that eliminate employing various production steps. Plants contain metabolites like terpenoids, polyphenols, alkaloids, and phenolic acids which play important roles in the bio-reduction and stability of metal ions to produce NPs.[16,17] However, finding effective ways to purify and concentrate NPs

synthesized from whole plants remain a costly challenge.[17] Hence, the utilization of plants extracts from various parts of the plant, such as leaves, stems, roots, etc., has gained great significance because plants provide renewable and cost-effective resources for the synthesis of NPs. Moreover, plant-extract mediated synthesis produce higher NP yields, are easy to purify, synthesis parameters are controllable, and easy to up-scale.[18,19]

Persea americana (avocado) is one of the largest fruit crops in the world with an estimated global production of over 50.4 million tonnes.[20] Majority of avocado produced either as fresh fruit or avocado processed products such as guacamole, avocado oil, and flavoring agents are for human consumption.[21] These products are derived from the mesocarp, while the peels and seeds are regarded as waste with no commercial use.[22] The avocado seed is a well-known repertoire of interest with highly valuable phytochemicals and have been proven to have antimicrobial, antioxidant, anti-inflammatory, and anticancer activities.[23−26] Despite these therapeutic potential uses, avocado seed still remains an under-utilized resource and a waste problem for the avocado industry.[27] Moreover, due to the large amounts of avocado seeds produced annually, there is a need to find alternative uses for this agro-waste product and reduce its associated environmental burden. Therefore, the aim of this study was to synthesize AuNPs using an aqueous avocado seed extract (AvoSE) and to evaluate their anticancer, antioxidant, and catalytic activities.

2. MATERIALS AND METHODS

2.1. Preparation of AvoSE. Fresh avocados were purchased from a local fruit market (Bellville Market, Cape Town, South Africa), and their seeds were isolated. The seeds were left to dry at room temperature for 3 months. Thereafter, the dried seeds were ground into fine powder using a blender. A 10% AvoSE was prepared by mixing 10 g of powder with 100 mL of distilled deionized water (ddH_2O). The mixture was heated in a microwave until boiling and then left stirring at 1000 rpm overnight at 25 °C. Afterward, the mixture was centrifuged at 9000 rpm at 4 °C for 10 min and the supernatant was vacuum filtered through Whatman no. 1 filter paper. The filtrate was frozen at −80 °C and freeze-dried using a FreeZone 25 L freeze dryer (Labconco, Kansas City, MO, USA). The dried extracts were wrapped in aluminum foil and stored at room temperature in a desiccator until needed.

2.2. Optimization of Reaction Conditions for the Synthesis of AuNPs Using AvoSE. Optimization of AuNP synthesis using aqueous AvoSE was done to obtain NPs (AvoSE−AuNPs) with tunable size and morphology. AvoSE−AuNPs were synthesized by mixing AvoSE and $HAuCl_4 \cdot 3H_2O$ at a volume ratio of 1:9 in 2 mL Eppendorf tubes. AvoSE−AuNPs' formation was indicated a by color change from light yellow to wine red/purple. Various parameters, such as temperature (25, 37, 50, 80, and 100 °C), pH (4, 5, 5.74, 6, 7, 8, 9, and 10), concentration of AvoSE (0.5, 1, 2, 4, 8, 16, 32, and 64 mg/mL), concentration of gold salt (0.25, 0.5, 0.75, 1, 2, 3, 4, and 5 mM), and reaction time (0−60 min) were optimized for the synthesis of AvoSE−AuNPs. All reactions were shaken on an orbital shaker (Eppendorf Thermomixer Comfort, Hamburg, Germany) at 1000 rpm. The AvoSE−AuNPs were centrifuged at 14,000 rpm for 15 min. The pellets were re-suspended in a volume of ddH_2O that is equal to the volume of the synthesis reaction. The washing was repeated two more times as above.

2.3. AvoSE−AuNP Characterization. The spectra of AvoSE−AuNPs were determined using a POLARstar Omega microplate reader (BMG Labtech, Offenburg, Germany) at a wavelength range of 400−800 nm. The hydrodynamic diameter, poly-dispersity index (PDI), and zeta potential (ζ-potential) of AuNPs were determined using a Nano-ZS90 Zetasizer instrument (Malvern Instruments Ltd., Malvern, UK) at a scattering angle of 90° at 25 °C. The morphology and size of the AvoSE−AuNPs were determined using a FEI Tecnai G^2 20 field-emission gun HRTEM (Hillsboro, OR, USA) operated in bright field mode at an accelerating voltage of 200 kV. Fourier transform infrared (FTIR) analysis was performed to determine the functional groups in AvoSE and AvoSE−AuNPs using the PerkinElmer Spectrum One FTIR spectrophotometer (Waltham, MA, USA). The AvoSE and AvoSE−AuNP dried samples were mixed with KBR and scanned on FTIR over the range of 4000−400 cm^{-1} at 2 cm^{-1} resolution.

2.4. Phytochemical and Antioxidant Activities of AvoSE and AvoSE−AuNPs. AvoSE (1 mg/mL) and AvoSE−AuNPs (0.017 mg/mL) were investigated for the presence of flavanols, flavonols, and polyphenols; as well as their antioxidant capacity, namely, ferric reducing antioxidant power (FRAP), oxygen radical absorbance capacity (ORAC), and 2,2-diphenyl-1-picrylhydrazyl (DPPH), using previously reported standard biochemical methods.[28]

2.4.1. Flavonol Content. The flavonol content in AvoSE and AvoSE−AuNPs were determined according to Mazza et al.[29] using quercetin (0, 5, 10, 20, 40, and 80 mg/L) as a reference standard. Briefly, 12.5 μL of samples were added in a 96-well plate and this was followed by the addition of 12.5 μL 0.1% HCl prepared in 95% ethanol and 225 μL of 2% HCl. The mixture was incubated for 30 min at room temperature and the absorbance was measured at 360 nm on a Multiskan SkyHigh microplate spectrophotometer (Thermo Fisher Scientific, Waltham, MA, USA). The flavonol content in the samples were expressed as milligram quercetin equivalent per gram of the sample (mgQE/g).

2.4.2. Flavanol Content. The flavanol content in AvoSE and AvoSE−AuNPs were determined according to Alabi et al.,[30] using catechin (0, 5, 10, 25, 50, and 100 μM) as a reference standard. Briefly, 25 μL of samples and 275 μL of 4-(dimethyamino)-cinnamaldehyde were dispensed into a 96-well plate and incubated for 30 min at room temperature. The absorbance of the mixture was read at 640 nm using a Multiskan SkyHigh microplate spectrophotometer. The flavanol contents in the AvoSE and AvoSE−AuNPs were expressed as mg catechin equivalent per gram (mgCatechin/g).

2.4.3. Total Phenolic Contents. The total phenolic contents of AvoSE and AvoSE−AuNPs were determined according to Waterhouse[31] using gallic acid (0, 20, 50, 100, 250, and 500 mg/L) as a reference standard. Briefly, 25 μg/mL samples were added into a 96-well plate followed by the addition of 125 μL Folin reagent and incubated for 5 min. Thereafter, 100 μL of 7.5% aqueous sodium carbonate was added to the mixture. The plate was incubated at room temperature for 2 h and the absorbance was measured at 765 nm using a Multiskan SkyHigh microplate spectrophotometer. The polyphenol content in the AvoSE and AvoSE−AuNPs were expressed as mg gallic acid equivalents (GAE) per dry mass of the sample (mgGAE/g).

2.4.4. ORAC Assay. The peroxyl-radical absorbing potential of antioxidants present in Avo-SE and AvoSE−AuNPs were measured according to Ou et al.[32] using Trolox (a water-

Scheme 1. AvoSE-Mediated Synthesis of AuNPs
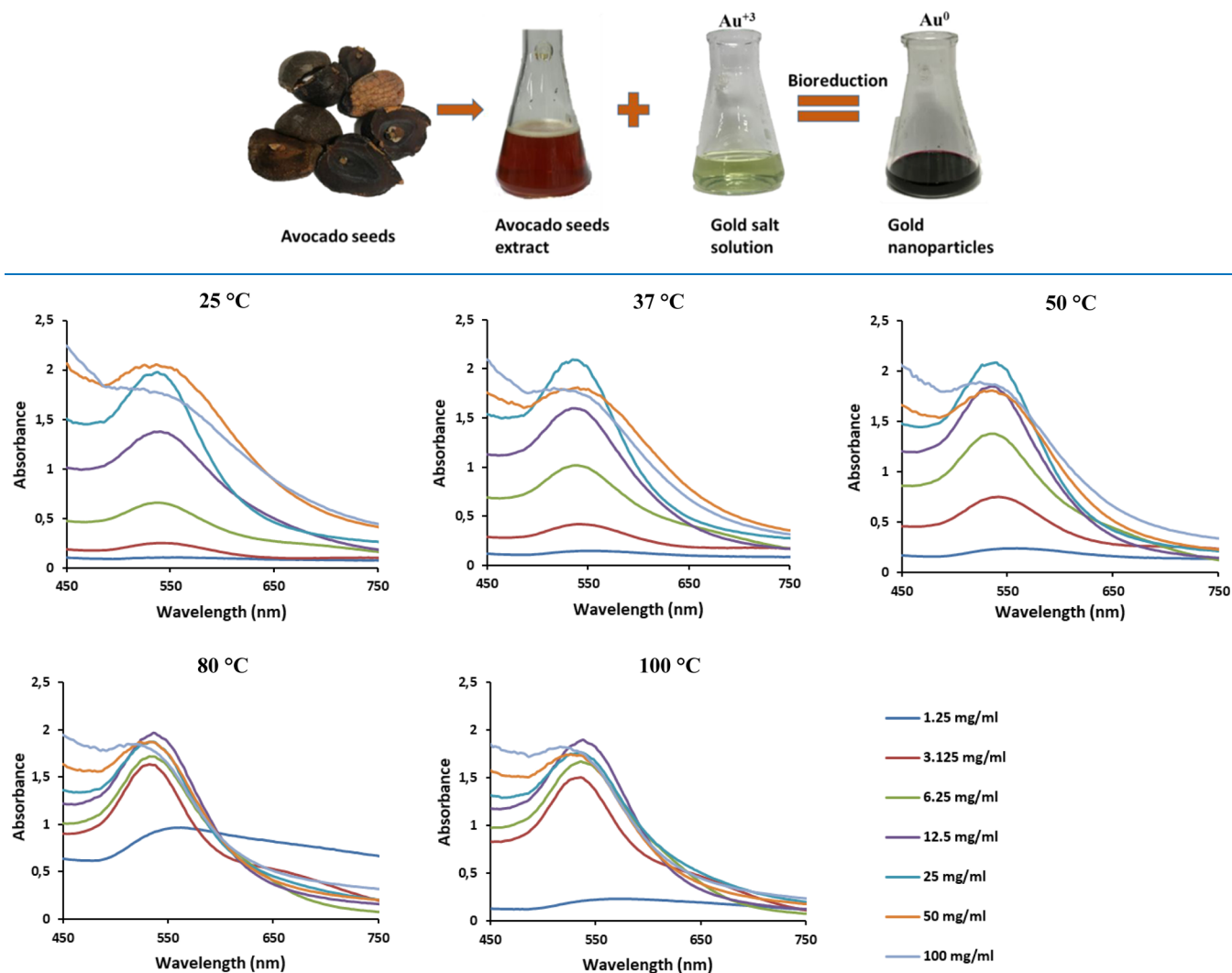

Figure 1. UV−vis spectra of AvoSE−AuNPs showing the effect of extract concentration and temperature on the synthesis.

soluble analogue of vitamin E) as a standard reference. Briefly, 12 μL of samples were dispensed in a 96-well plate, followed by 138 μL of 1.2 mM ORAC fluorescein solution and 50 μL of 2,2′-azobis (2-methylpropionamidine). The fluorescence intensity (485 ex/525 em) was monitored by a Fluoroskan Ascent microplate fluorometer (Thermo Fisher Scientific, Waltham, MA, USA) for 2 h at 1 min intervals. The results were expressed in micromoles of Trolox equivalents (TE) per liter of sample (μmolTE/L).

2.4.5. DPPH Assay. The DPPH radical scavenging ability of AvoSE and AvoSE−AuNPs was determined according to Lim and Lim,[33] using Trolox as the reference standard. Briefly, 10 μL of samples and 300 μL of DPPH reagent were added into a 96-well plate. The mixture was incubated for 30 min at room temperature and the absorbance was measured at 734 nm using a Fluoroskan Ascent microplate fluorometer. The results were expressed as μmolTE/L.

2.4.6. FRAP Assay. The ferric reducing power of AvoSE and AvoSE−AuNPs was determined according to the method of Benzie and Strain[34] using ascorbic acid as a reference standard. Briefly, 10 μL of samples were mixed with 300 μL of FRAP reagent into a 96-well plate and incubated for 30 min at room temperature. The absorbance was taken measured at 593 nm

using a Fluoroskan Ascent microplate fluorometer, and the results were expressed as micromoles of ascorbic acid equivalents (AAE) per liter of sample (μmolAAE/L).

2.5. In Vitro Cytotoxic Effect of AvoSE−AuNPs.
2.5.1. Cell Culture. Human colon (Caco-2) and prostate (PC-3) cancer cell lines were purchased from the American Type Culture Collection (Manassas, VA, USA). Caco-2 and PC-3 cells were cultured in Dulbecco's modified Eagle's medium and RPMI-1640 (Gibco, Roche, Germany), respectively, supplemented with 10% FBS (Gibco, Roche, Germany) and 1% pen−strep (Gibco, Roche, Germany). The cells were cultured at 37 °C in a humidified 5% CO_2 incubator.

2.5.2. Cytotoxic Effects of AvoSE−AuNPs Using the MTT Assay. Effects of the AvoSE−AuNPs on Caco-2 and PC-3 cells were determined using the MTT reagent following a previous protocol with slight modifications.[35] Caco-2 and PC-3 cells were individually seeded into sterile 96-well microplates at a density of 1×10^5 cells/mL, and incubated at 37 °C for 24 h. Afterward, the growth medium was replaced with 100 μL of either AvoSE−AuNPs or 5% dimethyl sulfoxide (Kimix, Cape Town, South Africa) as a positive control or growth medium as negative control and further incubated for 24 h. Then, 10 μL of MTT reagent (5 mg/mL MTT) was added in each well and

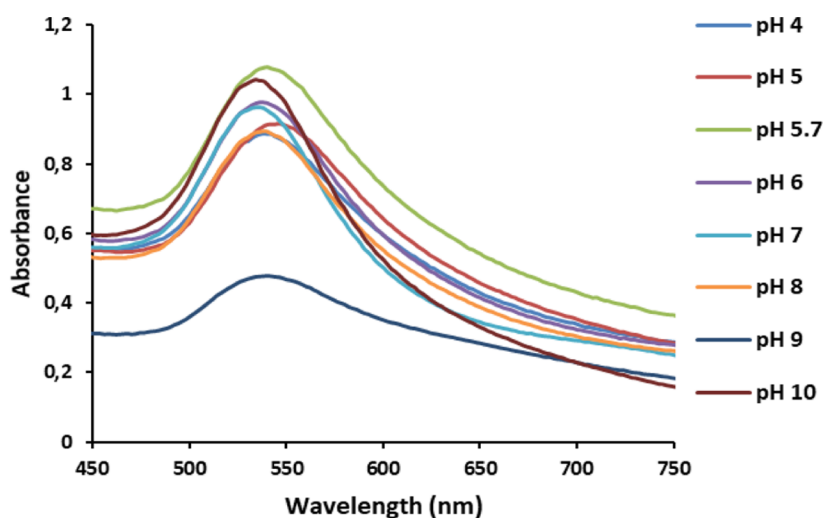**Figure 2.** UV−vis spectra of AvoSE−AuNPs showing the effect of pH on AvoSE−AuNPs' synthesis.
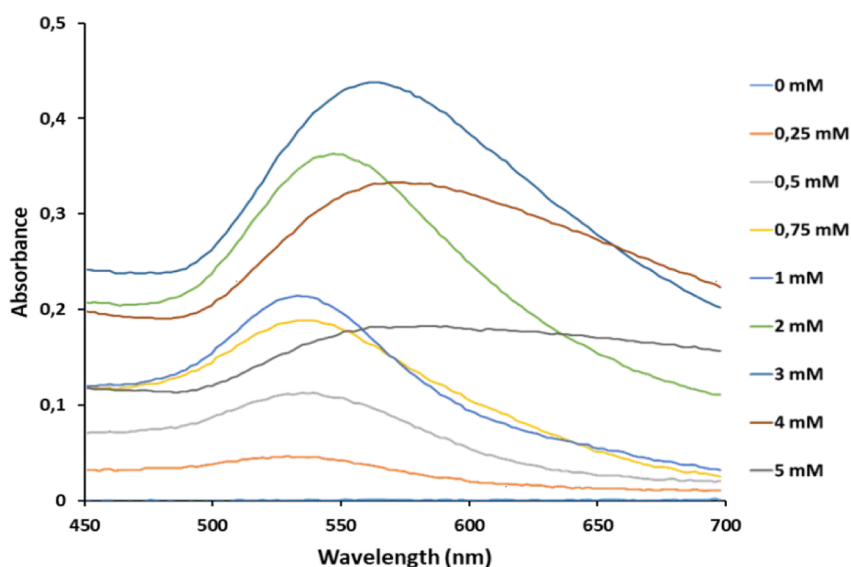

Figure 3. UV−vis spectra of AvoSE−AuNPs showing the effect of gold salt concentration on AvoSE−AuNPs' synthesis.

the plates were incubated for a further 3 h at 37 °C. The MTT−medium mixture was aspirated, replaced with 100 μL of dimethyl sulfoxide, and incubated for 30 min. The absorbance was measured on a POLARstar Omega microplate reader at 570 nm and a reference wavelength of 700 nm. Percentage cell viability was calculated in reference to the negative control.

2.6. Catalysis. *2.6.1. Catalytic Activity of AvoSE−AuNPs.* To investigate whether AvoSE−AuNPs have catalytic activity, the reduction of 4-nitrophenol (4-NP) in the presence of the biogenic AuNPs and NaBH$_4$ was performed following previous methods.[36−38] The absorption spectra of the reactions were read at a range of 270−700 nm using a POLARstar Omega microplate reader.

2.6.2. Reuse of AvoSE−AuNPs for 4-NP Reduction. To monitor the effects of the reusability of AvoSE−AuNPs on the reduction reaction, a similar method was used as above. After each 1 h cycle, the reaction solution was centrifuged at 14,000 rpm for 10 min at 25 °C. The supernatant was discarded and the pellet was re-suspended in 30 μL of ddH$_2$O. The reduction reaction was conducted as described above using the same AvoSE−AuNPs. This was repeated four more times.

2.6.3. Hydroxyl Radical Confirmation as Active Species Generated during Catalytic Reduction by AvoSE−AuNPs. The hydroxyl radical (•OH) species generated during the catalytic reduction of 4-NP were analyzed using isopropyl alcohol (IPA). The procedure was similar to the catalytic activity (Section 2.6.1), except that 10 or 25% IPA (30 or 75 μL) was added to the reaction prior to addition of NaBH$_4$.

3. RESULTS AND DISCUSSION

3.1. Synthesis of AvoSE−AuNPs. AuNPs were prepared by a plant extract-mediated method using AvoSE. Aqueous AvoSE was added to HAuCl$_4$ and the bio-reduction reaction was indicated by a visible color change (Scheme 1). The AvoSE, which exhibited an orange color, was mixed with the pale yellow HAuCl$_4$ aqueous solution (1 mM) and a rapid color change from pale yellow to purple occurred, indicating the formation of AuNPs from the Au^{3+} precursor.[39,40] The color change is attributed to the SPR which is due to the collective oscillation of electrons of AuNPs in resonance with light.[41]
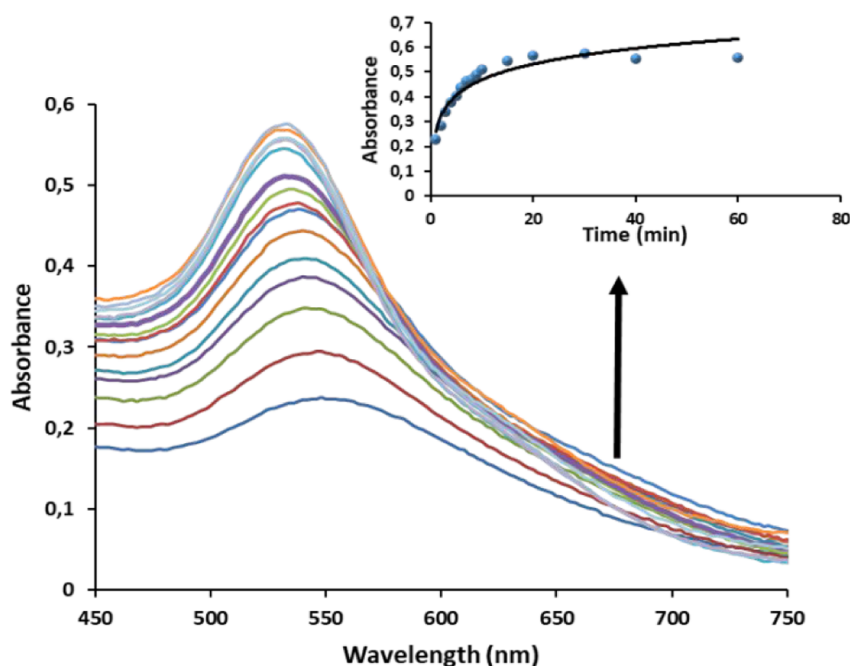
Figure 4. UV−vis spectra of AvoSE−AuNPs showing the effect of synthesis time on AvoSE−AuNPs' synthesis. Inset: absorbance of AvoSE−AuNPs at 530 nm over time.

3.2. Characterization of the Biogenic AvoSE−AuNPs.

3.2.1. UV−Vis Analysis. The formation of AvoSE−AuNPs was monitored by both changes in color and the appearance of the SPR peak on the UV−vis spectrum. Typically, the SPR peak for AuNPs occurs in the 500−580 nm range[30] and its width and position are strongly determined by several factors such as size, morphology, and surface features. These properties can be fine-tuned and improved by altering reaction parameters including temperature, pH, extract, and gold salt concentrations during synthesis.[42] Therefore, detailed investigation of the effects of various reaction conditions such as extract concentration, temperature, pH, gold salt concentration, and reaction time were conducted to investigate their effects on the AvoSE−AuNP synthesis.

(a) Effect of plant extract concentration and temperature on AvoSE−AuNP synthesis

As shown in Figure 1, the reduction of Au^{3+} into Au^0 by AvoSE and the formation of AvoSE−AuNPs was evidenced by the UV−vis spectra for all AvoSE concentrations and temperatures. AuNPs synthesized with 1.56 mg/mL AvoSE had a low absorbance which could be attributed to insufficient amount of reducing agents available to react with Au^{3+} present in solution, resulting in a low synthesis yield. The reaction containing 3.125 and 6.25 mg/mL AvoSE displayed broad SPR wavelength ranging between 554 and 568 nm, which indicated the formation of larger and anisotropic AuNPs.[43−45] Interestingly, 12.5 mg/mL AvoSE produced SPR peaks that are narrow, sharp, and symmetrical, indicating the formation of smaller AuNPs. Although reactions containing 25 mg/mL AvoSE exhibited similar results to the synthesis at 12.5 mg/mL, the SPR peaks were slightly broader compared to 12.5 mg/mL AvoSE. A rapid color change was observed for mixtures containing 50 and 100 mg/mL AvoSE; however, the SPR peaks were broad, indicating that the NPs may be polydisperse, anisotropic, and large in size.[45] This may be due to the presence of much higher amount of reducing agents as

compared to the amount of Au^{3+} present in solution. Hence, 12.5 mg/mL of AvoSE was selected as the optimum AvoSE concentration for the synthesis of AvoSE−AuNPs.

The effect of temperature on the synthesis of AvoSE−AuNPs was also investigated. The results indicated that the absorbance maximum obtained for AvoSE−AuNPs synthesized at AvoSE concentrations between 1.56 and 12.5 mg/mL increased with an increase in temperature, indicating a higher synthesis yield. Interestingly, the AuNP synthesized using 12.5 mg/mL AvoSE at 80 °C had distinct and narrow SPR peaks; thus, indicating the synthesis of smaller NPs, which may be attributed to the faster reaction rate at higher temperatures.[46] High temperatures increase the kinetic energy of molecules, and this promotes the fast reduction of Au^{3+}, hence reducing the probability for large particle size growth. A slight reduction in the absorbance was observed at 100 °C and this may be an indication that AuNPs synthesized using AvoSE require heat activation, but up to a certain point. Additionally, when the temperature is raised to a particular level and the number of NPs increases, the likelihood of NPs adhering to one another will also increase, resulting in larger AuNPs. This will result in a decrease in the adsorption of AuNPs on the SPR.[38,47] Therefore, 80 °C was chosen as the optimum temperature.

(b) Effect of pH on AvoSE−AuNP synthesis

The pH of the solution is another crucial factor that has an effect on the formation of AuNPs. It is well known that pH has the ability to change the charge of biomolecules, thus impact both their capping/stabilizing properties, and subsequently affect the shape and size of the particles.[46,48] As shown in Figure 2, AuNPs synthesized at pH range of 4−6 and at pH 8 and 9 had broad SPR peaks at a wavelength ranging between 538 and 546 nm, indicating that the synthesized AvoSE−AuNPs were polydispersed. AuNPs produced at pH 7 and 10 exhibited SPR peaks at 534 nm. However, AuNPs at pH 7 exhibited a sharp and narrow SPR peak which indicated the formation of smaller AvoSE−AuNPs. At higher pH values, the
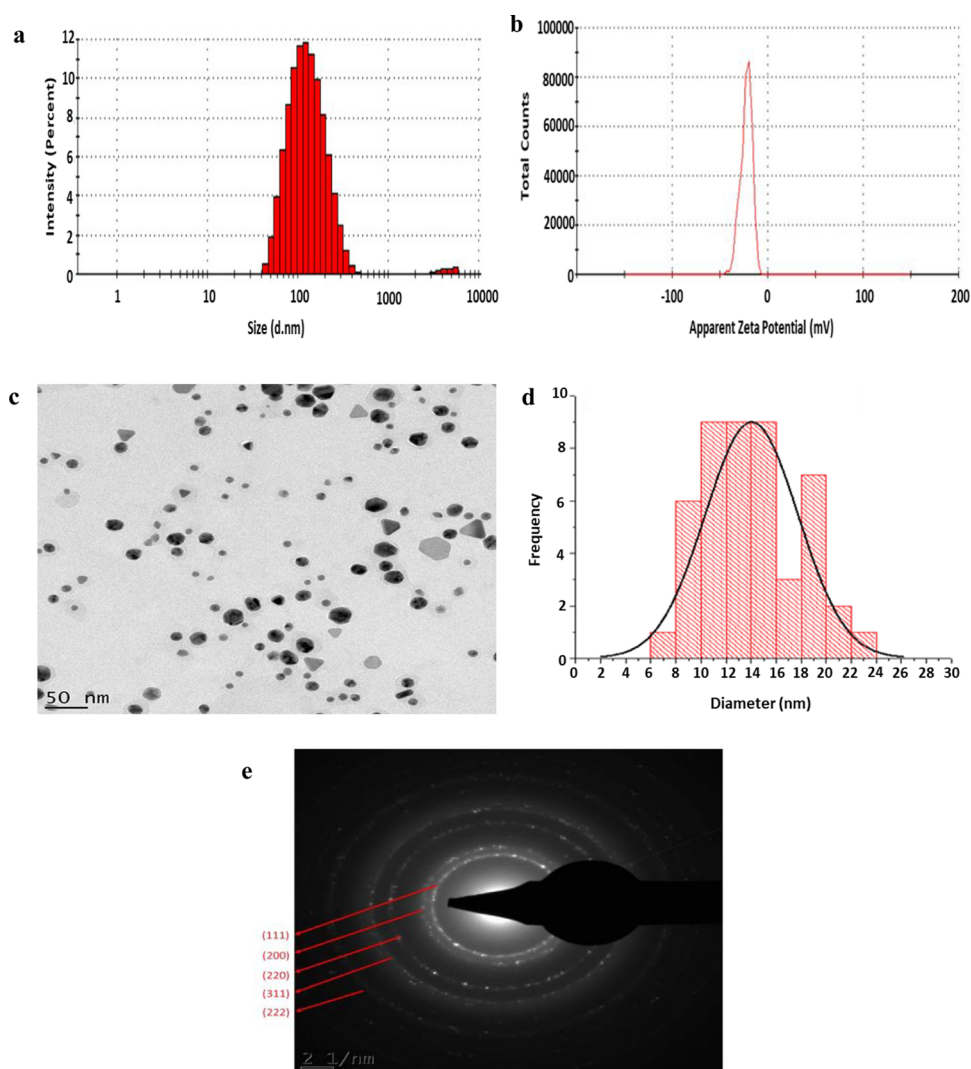
Figure 5. Characterization of the scaled-up AvoSE−AuNPs. (a) Size distribution, (b) zeta potential, (c) a representative TEM photomicrograph, (d) histogram showing the size distribution, and (e) SAED patterns of the synthesized AvoSE−AuNPs.
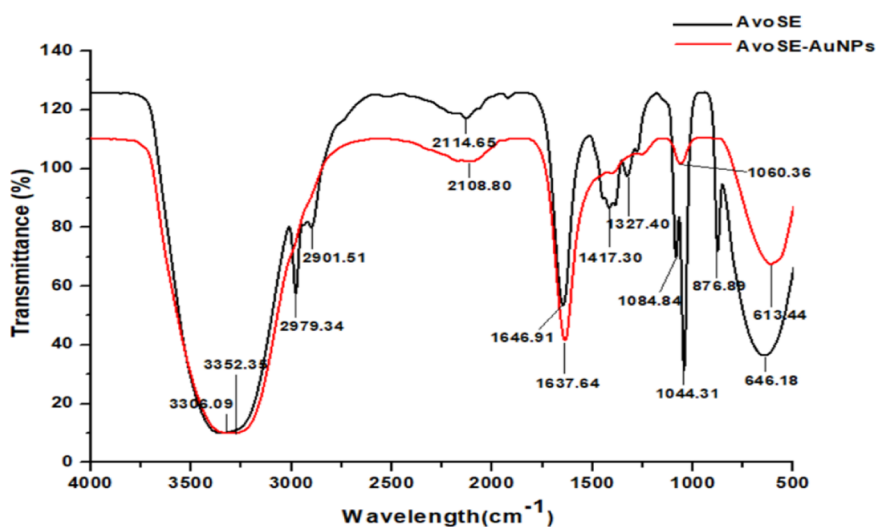
Figure 6. Representative FTIR spectra of AvoSE and AvoSE−AuNPs.

large number of phenolic functional groups available for gold binding facilitated a higher number of Au^{3+} to bind and subsequently form a large number of NPs with smaller diameters.[46] Therefore, in this study, the optimum pH chosen for the synthesis was pH 7. These results are in agreement with

Table 1. Characterized IR Absorptions from the FTIR Spectrum of AvoSE and AvoSE−AuNPs

peak position in extract (cm^{-1})	peak position in AuNPs (cm^{-1})	shift in position	type of chemical bond
3352.36	3306.09	+46.27	−OH, −NH
2114.65	2108.8	+5.85	C≡C
1646.91	1637.64	+9.27	−NH
1044.31	1060.36	−16.05	C−N
646.18	613.44	+32.74	C−Br

Table 2. Phytochemical Analysis and Antioxidant Capacity of AvoSE and AvoSE−AuNPs

phytochemical/antioxidant activity	AvoSE	AvoSE−AuNPs
flavonols (mgQE/g)	0.0189 ± 0.0013	0.2147 ± 0.0008
flavanols (mgCatechin/g)	0.0595 ± 0.0012	0
polyphenols (mgGAE/g)	92.2178 ± 0.0147	0
ORAC ($\mu molTE/L$)	65.9252 ± 4.2423	1822.015 ± 12.6338
DPPH ($\mu molTE/L$)	7.4927 ± 0.0244	128.7942 ± 0.0159
FRAP ($\mu molAAE/L$)	533.8856 ± 0.0191	343.8705 ± 0.0010

reported studies that the addition of hydroxide ions assists in the reduction reaction of metal ions.[49,50]

(c) Effect of HAuCl$_4$ on AvoSE−AuNP synthesis

The possibility of controlling the particle size and formation of NPs were further investigated by changing the concentration of HAuCl$_4$ (Figure 3). AvoSE−AuNPs produced using 0.25 and 0.5 mM HAuCl$_4$ exhibited broad SPR peaks with low

absorbances, which indicated that AvoSE−AuNPs' formation was not favorable at these concentrations. Narrow, sharp, and symmetrical spectra (at 536 nm) were formed at 0.75 and 1 mM HAuCl$_4$. At higher HAuCl$_4$ concentrations (2 and 3 mM), the spectra showed NP formation; however, the wavelengths were at 548 and 562 nm, respectively. The redshift suggested that these AvoSE−AuNPs could be anisotropic and large. The spectra for AuNPs produced with 4 and 5 mM HAuCl$_4$ were broad, with lower absorbances. This was likely due to excess gold ions present in proportion to reducing agents, which resulted in competition for reducing agents and hindered AuNPs nucleation. The results are in accordance with other studies, where biosynthesis of NPs increased with the increase in ion salt concentration.[49,51] Therefore, 1 mM HAuCl$_4$ was chosen as the optimum salt concentration for the synthesis of AvoSE−AuNPs.

### (d) Kinetics of AvoSE−AuNP synthesis

The kinetics of the AvoSE−AuNPs formation using the optimized conditions (12.5 mg/mL AvoSE, pH 7, 80 °C and 1 mM HAuCl$_4$) was studied in order to determine the rate of reaction and the optimum duration needed for the reduction to reach completion. As shown in Figure 4, the AvoSE−AuNP formation followed a rapid increase in the intensity of the spectra in the first 8 min and slowed down after 10 min. There was no significant change in absorbance after 30 min. This suggested that AvoSE−AuNP synthesis under optimum conditions is rapid and was completed within 30 min. The increase in absorbance at 530 nm over time (inset) indicated an increase in the synthesis yield. This is in accordance with
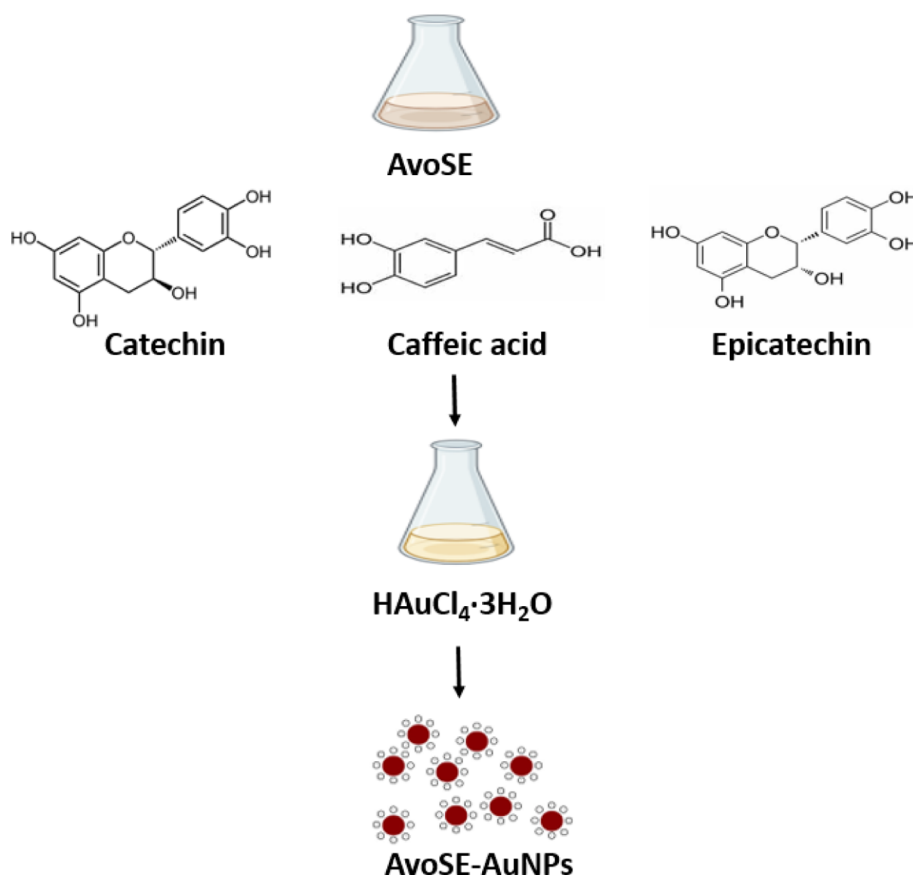
Figure 7. Possible mechanism of AvoSE−AuNPs' synthesis.
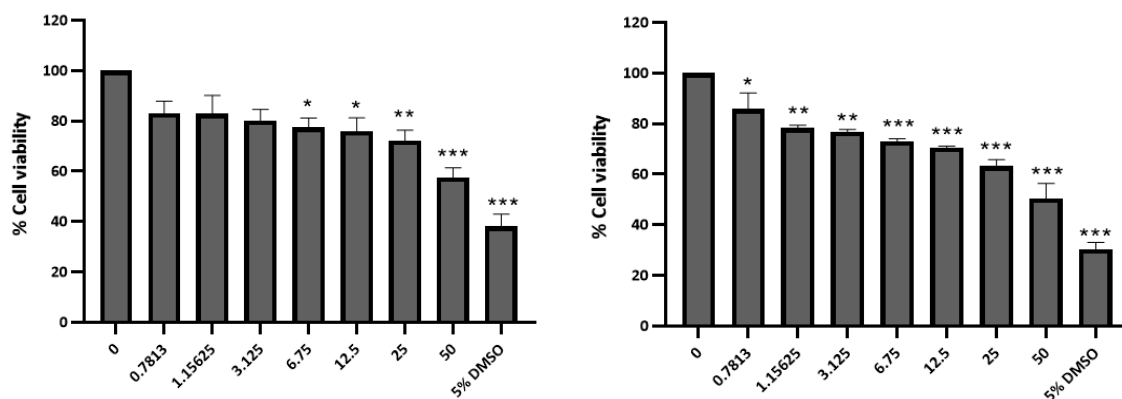
Figure 8. Cytotoxic effects of AvoSE−AuNPs on human cancer cell lines. The effect of AvoSE−AuNPs was tested on Caco-2 (a) and PC-3 (b) cells. Data are presented as the mean ± standard error mean (SEM) of three independent experiments performed in triplicate. Data were considered to be statistically significant when $***p < 0.001$, $**p < 0.01$, and $*p < 0.05$.
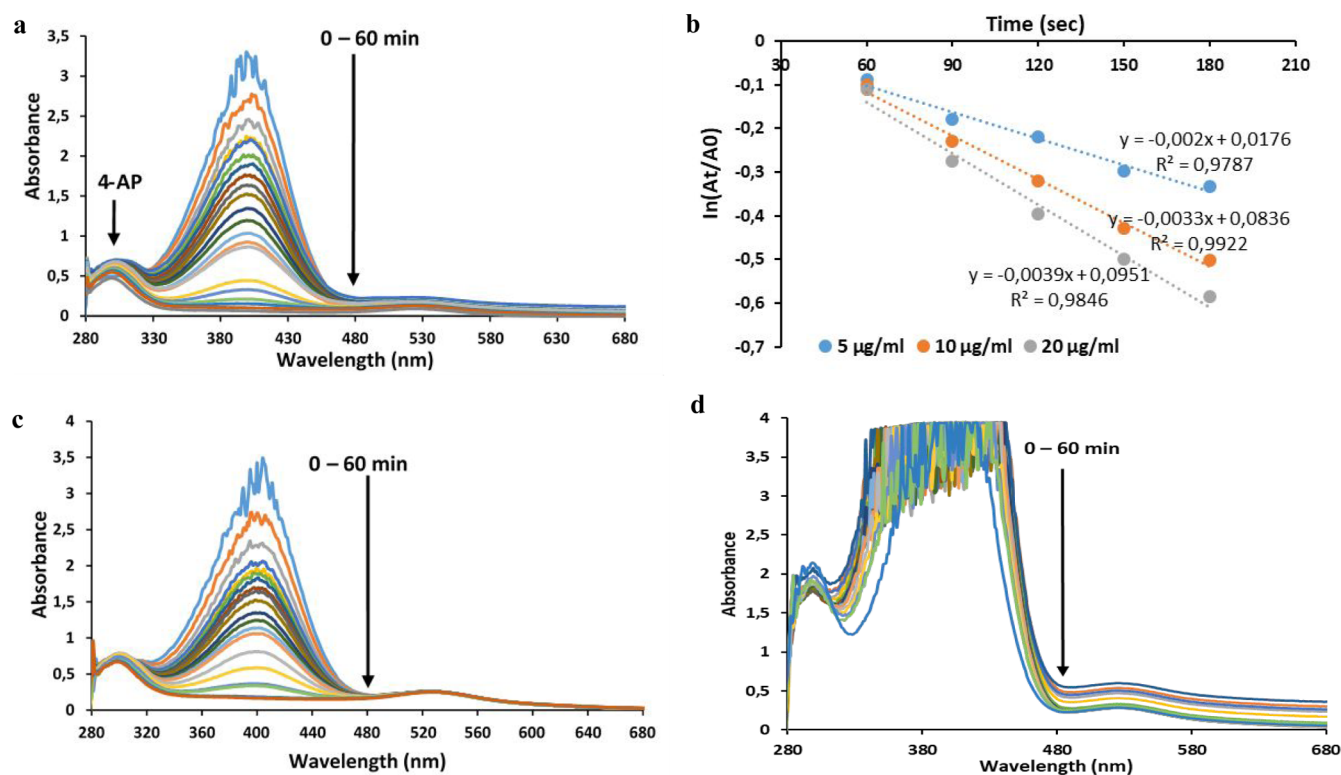

Figure 9. Catalytic activity of AvoSE−AuNPs (a) time-dependent UV−vis absorption spectra for the reduction of 4-NP in the presence of AvoSE−AuNPs and the gradual appearance of 4-AP over 60 min. (b) Plot of $\ln(A_t/A_0)$ vs time (min) for the catalytic conversion of 4-NP at varying concentrations of AvoSE−AuNPs and 4-NP. UV−vis absorption spectra for the reduction of 4-NPs at various 4-NP concentrations (c) 2 mM 4-NP and (d) 10 mM 4-NP.

previous studies which have demonstrated that the absorbance is directly proportional to the AuNP concentration or synthesis yield.[52,53] The rate of synthesis was found to be 0.3608 min^{-1}; further giving credence to the optimization done before the determination of the rate of synthesis and confirmed that nucleation was completed at 30 min. The reaction time in this study was found to be lower than several reported studies.[54−56] AvoSE−AuNPs were synthesized using the following optimal parameters: 12.5 mg/mL AvoSE, pH 7, 80 °C and 1 mM HAuCl$_4$ for 30 min.

3.2.2. DLS and TEM Analysis. Figure 5a,b shows the average hydrodynamic size (101.39 ± 1.4 nm), PDI (0.295 ± 0.02), and ζ-potential (−24.26 ± 0.99 mV) of the optimized AvoSE−

AuNPs. Thus, indicating that the NPs were mostly monodispersed and highly stable.[57,58] Transmission electron microscopy (TEM) images revealed that the AvoSE−AuNPs were anisotropic and predominantly spherical in shape (Figure 5c). The other shapes observed were hexagonal, triangular, and rod-shaped NPs.[45] In plant extract-mediated synthesis, different phytochemicals in the extracts are capable of reducing the Au^{3+} and give rise to anisotropic AuNPs.[59−61] No signs of aggregation was observed in this study, and this could be attributed to the presence of phytochemicals in the extract, which also acted as stabilizing agents during the biosynthesis.[62] This is further supported by the presence of a "halo" around the NPs. The AvoSE−AuNPs had an average core size of 14 ±
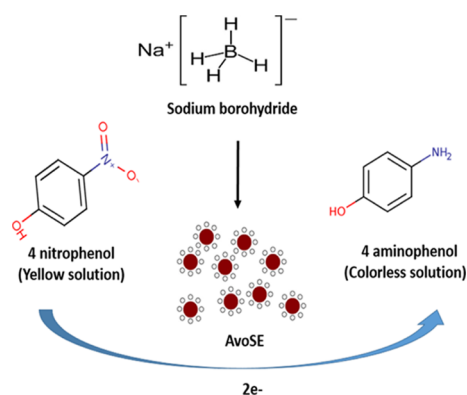
Figure 10. Possible mechanism of catalytic reduction of 4-NP.

3.7 nm (Figure 5d), which is significantly smaller than that measured by DLS (101.39 ± 1.4 nm). This variation may be attributed to the adsorption of organic stabilizers from the extract on the surface of AuNPs, and the hydrodynamic capacity of water on the stabilized AuNPs could have had an effect on the average particle hydrodynamic size obtained by the DLS.[63−65] Figure 5e shows the selected area electron diffraction (SAED) pattern, which confirms the crystalline nature of the AvoSE−AuNPs. The observed rings were found to correspond to the (111), (200), (220), (311), and (222) reflections of face centered cubic gold. The bright observed rings were indexed according to studies which reported similar results to that of biosynthesized AvoSE−AuNPs.[63,66]

3.2.3. FTIR Analysis. FTIR analyses of both the AvoSE−AuNPs and AvoSE were performed to identify the functional groups which are involved in the biosynthesis of the AvoSE−AuNPs. The results for FTIR analysis are shown in Figure 6, and the bonds that are involved in the formation of AvoSE−AuNPs are shown in Table 1. The FTIR spectra of AvoSE−AuNPs has broad absorption peak at 3305.09 cm^{-1} corresponding to the vibration of −OH and −NH stretching bonds which are due to the presence of alcohols, phenols, carboxylic acids, and primary/secondary amines.[67] The presence of a weak peak at 2108.8 cm^{-1} corresponds to the existing vibration of C≡C which is attributed to the presence of alkynes.[68,69] The absorption peaks at 1637.64 and 1060.36

cm^{-1} are attributed to the −NH bending and C−N stretching vibrations representing primary and aromatic amines,[70] respectively. Apart from the listed peaks, AvoSE−AuNPs also showed an absorption peak at 613.44 cm^{-1} which is primarily due to a C−Br stretch. These results are in accordance with several studies which have identified peaks at 3330, 3000−2840, 2920, 1730, 1580, and 1150−1000 cm^{-1} from raw avocado seeds.[71] The spectra indicated the presence of hydroxyl and carboxylic groups on the AvoSE−AuNPs, and this may possibly be a result of the involvement of flavonoids, terpenoids, phenolic compounds, and/or carbohydrates in the synthesis process. Several studies have reported the role of hydroxyl and carboxylic acids-containing compounds in the bio-reduction, capping, and stabilization of AuNPs.[72,73] Amino acids and proteins are also suggested to act as stabilizers of AuNPs after the reduction process.[74] The functional groups listed were identified on the AvoSE−AuNPs, and thus, we speculate their involvement in the synthesis of AvoSE−AuNPs. These data are corroborated by Bogireddy and Agarwal.[75]

3.3. Phytochemical and Antioxidant Analysis of AvoSE−AuNPs. The quantitative phytochemical content and antioxidant activity of aqueous AvoSE and AvoSE−AuNPs were investigated. As shown in Table 2, the comparative analysis showed that AvoSE revealed the presence of flavonols (0.0189 ± 0.0013 mgQE/g); flavanols (0.0595 ± 0.0012 mgCatechin/g); and polyphenols (92.2178 ± 0.0147 mgCatechin/g), while AvoSE−AuNPs showed higher flavonol contents (0.2147 ± 0.0008 mgQE/g) compared to AvoSE. No flavanol and polyphenol contents were detected. This suggests that the flavanols and polyphenols present in AvoSE may have been consumed during the reduction process leading to the synthesis of AvoSE−AuNPs. Avocado is a nutritious food that is rich in phytochemicals and the polyphenols are the most abundant. Major polyphenols that have been identified in AvoSE include catechin, caffeic acid, kaempferol, chlorogenic acid, and procyanidins.[76] These compounds are the major constituents of antioxidants and possess reducing properties necessary for the synthesis of NPs. Moreover, DPPH, ORAC, and FRAP anti-oxidant assays showed that both AvoSE and AvoSE−AuNPs have excellent antioxidant activity (Table 2). In comparison, AvoSE and AvoSE−AuNPs showed DPPH radical scavenging power of approximately 7.50 ± 0.0244 and
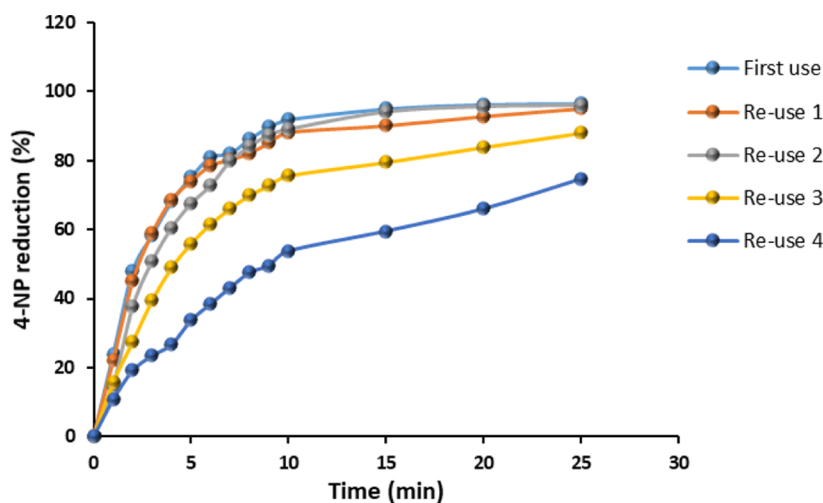
Figure 11. Reusability of 10 μg/mL AvoSE−AuNPs for the reduction of 4-NP with NaBH$_4$. The percentage catalytic activities of 4-NP in each cycle within 25 min were 96, 94, 95, 87, and 74%, respectively.
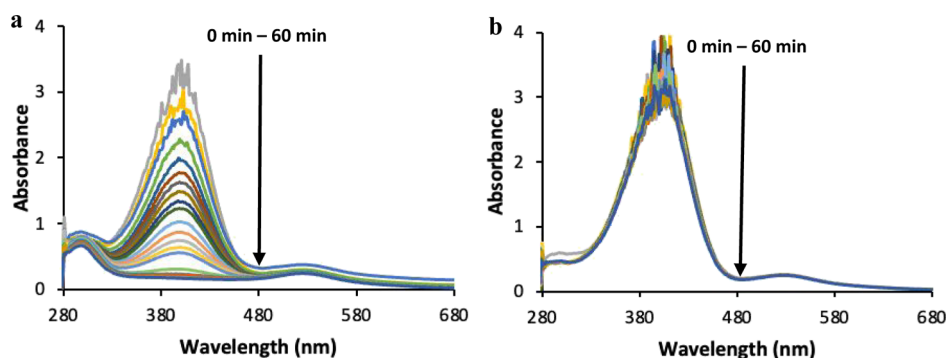
Figure 12. Effect of IPA concentration on the reduction kinetics of 4-NP in the presence of AvoSE−AuNPs. (a) No IPA and (b) 10% IPA.

128.80 ± 0.0159 μmolTE/L, ORAC antioxidant capacity of 65.93 ± 4.2423 and 1822.02 ± 12.6228 μmolTE/L, and FRAP of 533.89 ± 0.0191 and 343.88 ± 0.0010 μmolAAE/L, respectively. As expected, AvoSE−AuNPs exhibited higher antioxidant activity compared to AvoSE, and this could be due to the inclusion of antioxidants such as polyphenols and flavonoids as reductants of Au^{3+} for the formation of AuNPs.[77] The possible mechanism of the formation of AvoSE−AuNPs is shown in Figure 7.

3.4. In Vitro Cytotoxic Effects of AvoSE−AuNPs. Cell viability using the MTT assay was performed on Caco-2 and PC-3 cells following a 24 h exposure to increasing concentrations of AvoSE−AuNPs (0.78−50 μg/mL). Treatment with 5% DMSO served as a positive control. The results depicted in Figure 8 revealed that AvoSE−AuNPs and DMSO treatments caused a decrease in the viability of cells in comparison to untreated control. Figure 8a showed that lower concentrations (0.7813−3.125 μg/mL) of AvoSE−AuNPs had no effect on the viability of Caco-2 cells; however, significant reduction in cell viability was noted for concentrations ranging from 6.25 to 50 μg/mL. Interestingly, Caco-2 cells exposed to 50 μg/mL of AvoSE−AuNPs had a 58% cell viability rate, indicating that the AvoSE−AuNPs were toxic to Caco-2 cells only at higher concentrations. In contrast, the AvoSE−AuNPs showed a dose-dependent decrease in % viability of PC-3 cells (Figure 8b), with 0.7813 and 50 μg/mL showing 86 and 50% viability, respectively, indicating their higher sensitivity effect on PC-3 cells as compared to Caco-2 cells. Although this study suggests that AvoSE−AuNPs exhibited anticancer effects on both Caco-2 and PC-3, this effect was more pronounced in PC-3 cells. The inhibition of cell proliferation and reduction in cell viability of avocado seed has been well documented.[23,26,78] A study by Alkhalaf et al. revealed % decrease in cell proliferation of human liver (HepG2) and colon (HCT-116) cancer cells after treatment with lipid extract of avocado seeds.[23,27] Similarly, Dabas et al. demonstrated the cytotoxic effect of AvoSE on prostate (LNCaP), breast (MCF-7), lung (H1299), and colon (HT-29) cells with half maximal inhibitory concentrations ranging from 19 to 132 μg/mL following a 48 h treatment.[79] The anticancer properties of AvoSE are often credited to its constituent bioactive compounds, namely, tannins, phenolics, and flavonoids.[80] Therefore, the anticancer activity of AvoSE−AuNPs presented in this study could also be attributed to the bioactive compounds present in AvoSE, which were responsible for the formation of AvoSE−AuNPs.

3.5. Catalysis. *3.5.1. Catalytic Activity of AvoSE−AuNPs.* The catalytic reduction of 4-NP by AvoSE−AuNPs in the presence of NaBH$_4$ was also investigated in this study. The catalytic reduction reaction was initiated by the addition of NaBH$_4$ to 4-NP, which resulted in a color change from light-yellow to a bright yellowish-green color.[55] This color change showed the formation of 4-nitrophenolate ions, which is characterized by a shift in absorption peak from 321 to 400 nm (Figure S1a,b). The AvoSE did not show any catalytic activity when added to the 4-NP and NaBH$_4$ solution, and as a result, the 4-nitrophenolate peak remained unchanged up to 60 min, with no formation of 4-AP (Figure S1c). In contrast, the addition of AvoSE−AuNPs to the reaction resulted in the decrease of the 4-nitrophenolate peak over time; this was followed by the appearance and gradual increase of the peak at 300 nm (Figure 9a), indicating the formation of 4-AP.[36,81−83] This suggested that the catalytic reduction occurs rapidly and was completed within 45 min when using AvoSE−AuNPs.

Several studies have reported that the amount of nano-catalyst, the initial concentration of 4-NP, and NaBH$_4$ are important factors that influence the catalytic reduction of 4-NP to 4-AP by metal NPs.[84−86] Moreover, since the reaction kinetics is a pseudo-first order with respect to 4-NP concentration, an apparent reaction rate constant, k_{app}, was calculated from the linear slope of the $\ln(A_t/A_0)$ versus time plot, where A_t/A_0 is the nitrophenolate absorbance normalized to the absorbance at the start of the reaction. Therefore, to study the effect on k_{app}, experiments were carried out by varying the AvoSE−AuNPs and 4-NP concentration, with a constant NaBH$_4$ concentration. Figure 9b shows the plots of pseudo-first-order kinetics for the catalytic reduction of 4-NP using varying concentrations of AvoSE−AuNPs (5, 10 and 20 μg/mL). The rate constant for pseudo-first-order kinetics were found to be 3.9×10^{-3}, 3.3×10^{-3}, and 2×10^{-3} s^{-1} for 5, 10, and 20 μg/mL AvoSE−AuNPs, respectively. The results indicated that the rate of 4-NP reduction was correspondingly increased with the increase in the concentration of the AvoSE−AuNPs. A study by Bogireddy and Agarwal revealed a k_{app} of 1.55×10^{-3} s^{-1} when using 30 μg/mL AvoSE−AuNPs at 10 mM NaBH$_4$,[75] further corroborating the ability of AvoSE−AuNPs in reducing 4-NP.

Figure 9c,d shows the spectra for the catalytic reduction of 4-NP using 2 and 10 mM 4-NP, respectively. The k_{app} for 2 mM 4-NP was found to be 5.5×10^{-3} s^{-1}, indicating a high 4-NP reduction rate at this concentration. The results indicated that the reduction of 4-NP was slow at increased concentration, which is attributable to a high kinetic barrier. It has always been assumed that the adsorption of molecules onto the NPs surface is fast and reversible, and that the co-adsorption of 4-NP and NaBH$_4$ is required because all steps of

this reaction proceed only on the surface of the NPs, in accordance with the Langmuir−Hinshelwood model.[87] However, when the initial 4-NP concentration in solution is high, the active sites are mostly occupied by 4-NP molecules and a minority by active hydrogen species, which result in a low velocity constant of the reaction.[84] In contrast, as the surface area increases and the initial concentration of 4-NP remains constant or decreases, fewer 4-NP molecules adsorb on the surface because the majority of active sites are occupied by active hydrogen species, which lead to the increasing reaction velocity.[84,88] According to Neal and colleagues, in this catalysis reaction, the 4-NP ion (i.e., nitrophenolate) is first adsorbed onto the catalyst (AuNPs) where it is then reduced to 4-AP (or 4-aminophenolate) by a hydrogen species derived from BH_4^-. They further suggested that the overall process sees two oxygen atoms on the 4-NP ion replaced with two hydrogen atoms to yield the 4-AP product. The 4-AP, once generated, is rapidly desorbed from the surface of the AuNPs.[89] The possible mechanism of catalytic action of AvoSE−AuNPs is shown in Figure 10.

3.5.2. Reuse of AvoSE−AuNPs for 4-NP Reduction. The presence of a peak at ∼530 nm (Figure S2) showed that the AuNPs have not been transformed in the reaction and were still intact, thus indicating that they can be used in another cycle. Therefore, in order to evaluate the recyclability of the catalyst, the NPs were recovered by centrifugation and reused as catalysts in other reactions. The 5 μg/mL AvoSE−AuNPs were recyclable and used up to four times (Figure S3), whereas the 10 μg/mL AvoSE−AuNPs was used up to five times (Figure S4). Although the catalytic activity slightly decreased during cycles for 10 μg/mL AvoSE−AuNPs, the % catalytic reduction of 4-NP to 4-AP exceeded 74% after being used for five times (Figure 11). The results confirmed that the AvoSE−AuNPs exhibited good stability and recyclability during the catalytic reduction of 4-NP. This is important as some of the main concerns regarding the use of metallic NPs as catalysts lies within the cost effectiveness, recovery, and reusability of the recovery and reusability of the catalyst.[90,91]

3.5.3. Hydroxyl Radical Confirmation. To ascertain the role of hydroxyl radical requirement for the catalytic reduction mechanism, an oxidizing agent, IPA, was used as a scavenger.[92] As illustrated in Figure 12, when the 4-NP reduction was performed in the presence of 10% IPA, only 5% of 4-NP was reduced, compared to 94% degradation in the reaction without IPA. It has previously been shown that the reduction kinetics is strongly affected by the presence of alcohol in the reaction medium.[92] This study further corroborated other works showing that the hydroxyl radical is indeed the major reducing agent in the reduction of 4-NP to 4-AP.

4. CONCLUSIONS

This study investigated the antioxidant, anticancer, and catalytic activities of AvoSE−AuNPs. The optimized parameters for the synthesis of AvoSE−AuNPs were 12.5 mg/mL AvoSE, pH 7, 80 °C, 1 mM HAuCl$_4$ and 30 min synthesis time. The AvoSE−AuNPs were predominantly spherical in shape, displayed excellent antioxidant and significant anticancer activities, as well as high recyclable catalytic activity for the reduction of 4-NP to 4-AP. Overall, this study demonstrated that green synthesized AvoSE−AuNPs have potential usefulness as novel NPs in biological and environmental applications.

■ ASSOCIATED CONTENT

ⓈⒾ Supporting Information

The Supporting Information is available free of charge at https://pubs.acs.org/doi/10.1021/acsomega.3c02260.

> UV−vis spectra, catalytic activity of AvoSE-AuNPs, reusability of 5 μg/mL AvoSE−AuNPs for the reduction of 4-NP to 4-AP, and reusability of 10 μg/ml AvoSE−AuNPs for the reduction of 4-NP to 4-AP (PDF)

■ AUTHOR INFORMATION

Corresponding Author

Abram M. Madiehe − *Nanobiotechnology Research Group, Department of Biotechnology and DSI/Mintek Nanotechnology Innovation Centre, Biolabels Node, Department of Biotechnology, University of the Western Cape, Bellville 7535, South Africa*; Email: amadiehe@uwc.ac.za

Authors

Yonela Ngungeni − *Nanobiotechnology Research Group, Department of Biotechnology and DSI/Mintek Nanotechnology Innovation Centre, Biolabels Node, Department of Biotechnology, University of the Western Cape, Bellville 7535, South Africa*

Jumoke A. Aboyewa − *DSI/Mintek Nanotechnology Innovation Centre, Biolabels Node, Department of Biotechnology, University of the Western Cape, Bellville 7535, South Africa*

Koena L. Moabelo − *Nanobiotechnology Research Group, Department of Biotechnology and DSI/Mintek Nanotechnology Innovation Centre, Biolabels Node, Department of Biotechnology, University of the Western Cape, Bellville 7535, South Africa*; ⓞ orcid.org/0000-0002-9114-4530

Nicole R. S. Sibuyi − *DSI/Mintek Nanotechnology Innovation Centre, Biolabels Node, Department of Biotechnology, University of the Western Cape, Bellville 7535, South Africa*; ⓞ orcid.org/0000-0001-7175-5388

Samantha Meyer − *Department of Biomedical Sciences, Faculty of Health and Wellness Sciences, Cape Peninsula University of Technology, Bellville 7535, South Africa*

Martin O. Onani − *Organometallics and Nanomaterials, Department of Chemical Sciences, University of the Western Cape, Bellville 7535, South Africa*; ⓞ orcid.org/0000-0002-4735-3669

Mervin Meyer − *DSI/Mintek Nanotechnology Innovation Centre, Biolabels Node, Department of Biotechnology, University of the Western Cape, Bellville 7535, South Africa*

Complete contact information is available at:
https://pubs.acs.org/10.1021/acsomega.3c02260

Notes

The authors declare no competing financial interest.

■ REFERENCES

(1) Montazer, M.; Harifi, T. 2-Nanofinishing: fundamental principles. In *Nanofinishing of Textile Materials*; Woodhead Publishing, 2018; pp 19−34.

(2) Brainina, K.; Stozhko, N.; Bukharinova, M.; Vikulova, E. Nanomaterials: Electrochemical properties and application in sensors. *Phys. Sci. Rev.* 2018, 3, 20188050.

(3) Hammami, I.; Alabdallah, N. M.; jomaa, A. A.; kamoun, M. Gold nanoparticles: Synthesis properties and applications. *J. King Saud Univ., Sci.* 2021, 33, 101560.

(4) Siddique, S.; Chow, J. C. Gold nanoparticles for drug delivery and cancer therapy. *Appl. Sci.* 2020, 10, 3824.

(5) Jamkhande, P. G.; Ghule, N. W.; Bamer, A. H.; Kalaskar, M. G. Metal nanoparticles synthesis: An overview on methods of preparation, advantages and disadvantages, and applications. *J. Drug Delivery Sci. Technol.* 2019, 53, 101174.

(6) Pechyen, C.; Ponsanti, K.; Tangnorawich, B.; Ngernyuang, N. Waste fruit peel−Mediated green synthesis of biocompatible gold nanoparticles. *J. Mater. Res. Technol.* 2021, 14, 2982−2991.

(7) Jimenez, E.; Abderrafi, K.; Abargues, R.; Valdes, J. L.; Martinez-Pastor, J. P. Laser-ablation-induced synthesis of SiO2-capped noble metal nanoparticles in a single step. *Langmuir* 2010, 26, 7458−7463.

(8) Noruzi, M.; Zare, D.; Khoshnevisan, K.; Davoodi, D. Rapid green synthesis of gold nanoparticles using Rosa hybrida petal extract at room temperature. *Spectrochim. Acta, Part A* 2011, 79, 1461−1465.

(9) Singh, J.; Dutta, T.; Kim, K.-H.; Rawat, M.; Samddar, P.; Kumar, P. 'Green'synthesis of metals and their oxide nanoparticles: applications for environmental remediation. *J. Nanobiotechnol.* 2018, 16, 84.

(10) Menon, S.; Rajeshkumar, S.; Kumar, S. A review on biogenic synthesis of gold nanoparticles, characterization, and its applications. *Resour.-Effic. Technol.* 2017, 3, 516−527.

(11) Lee, K. X.; Shameli, K.; Yew, Y. P.; Teow, S.-Y.; Jahangirian, H.; Rafiee-Moghaddam, R.; Webster, T. J. Recent developments in the facile bio-synthesis of gold nanoparticles (AuNPs) and their biomedical applications. *Int. J. Nanomed.* 2020, 15, 275−300.

(12) Tarannum, N.; Divya, D.; Gautam, Y. K. Facile green synthesis and applications of silver nanoparticles: a state-of-the-art review. *RSC Adv.* 2019, 9, 34926−34948.

(13) Some, S.; Kumar Sen, I.; Mandal, A.; Aslan, T.; Ustun, Y.; Yilmaz, E. Ş.; Katı, A.; Demirbas, A.; Mandal, A. K.; Ocsoy, I. Biosynthesis of silver nanoparticles and their versatile antimicrobial properties. *Mater. Res. Express* 2018, 6, 012001.

(14) Ocsoy, I.; Tasdemir, D.; Mazicioglu, S.; Celik, C.; Katı, A.; Ulgen, F. Biomolecules incorporated metallic nanoparticles synthesis and their biomedical applications. *Mater. Lett.* 2018, 212, 45−50.

(15) Korde, P.; Ghotekar, S.; Pagar, T.; Pansambal, S.; Oza, R.; Mane, D. Plant extract assisted eco-benevolent synthesis of selenium nanoparticles-a review on plant parts involved, characterization and their recent applications. *J. Chem. Rev.* 2020, 2, 157−168.

(16) Korde, P.; Ghotekar, S.; Pagar, T.; Pansambal, S.; Oza, R.; Mane, D. Plant extract assisted eco-benevolent synthesis of selenium nanoparticles-a review on plant parts involved, characterization and their recent applications. *J. Chem. Rev.* 2020, 2, 157−168.

(17) Saim, A. K.; Kumah, F. N.; Oppong, M. N. Extracellular and intracellular synthesis of gold and silver nanoparticles by living plants: A review. *Nanotechnol. Environ. Eng.* 2021, 6, 1.

(18) Stozhko, N. Y.; Bukharinova, M. A.; Khamzina, E. I.; Tarasov, A. V.; Vidrevich, M. B.; Brainina, K. Z. The effect of the antioxidant activity of plant extracts on the properties of gold nanoparticles. *Nanomaterials* 2019, 9, 1655.

(19) Rama, P.; Baldelli, A.; Vignesh, A.; Altemimi, A. B.; Lakshmanan, G.; Selvam, R.; Arunagirinathan, N.; Murugesan, K.; Pratap-Singh, A. Antimicrobial, antioxidant, and angiogenic bioactive silver nanoparticles produced using Murraya paniculata (L.) jack leaves. *Nanomater. Nanotechnol.* 2022, 12, 18479804211056167.

(20) Dymond, K.; Celis-Diez, J. L.; Potts, S. G.; Howlett, B. G.; Willcox, B. K.; Garratt, M. P. The role of insect pollinators in avocado production: A global review. *J. Appl. Entomol.* 2021, 145, 369−383.

(21) Caballero, B.; Finglas, P.; Toldrá, F. *Encyclopedia of Food and Health*; Academic Press, 2015.

(22) Domínguez, M. P.; Araus, K.; Bonert, P.; Sánchez, F.; San Miguel, G.; Toledo, M. The avocado and its waste: an approach of fuel potential/application. In *Environment, Energy and Climate Change II*; Springer, 2014; pp 199−223.

(23) Alkhalaf, M. I.; Alansari, W. S.; Ibrahim, E. A.; ELhalwagy, M. E. Anti-oxidant, anti-inflammatory and anti-cancer activities of avocado (Persea americana) fruit and seed extract. *J. King Saud Univ., Sci.* 2019, 31, 1358−1362.

(24) Dennis, C. N.; Savitri, W. Antibacterial effect of ethanol extract of the avocado seed (Persea Americana Mill.) as an alternative root canal Irrigants against Porphyromonas Gingivalis (In Vitro). *Int. J. Appl. Dent. Sci.* 2017, 31, 89−93.

(25) Villarreal-Lara, R.; Rodríguez-Sánchez, D. G.; Díaz De La Garza, R. I.; García-Cruz, M. I.; Castillo, A.; Pacheco, A.; Hernández-Brenes, C. Purified avocado seed acetogenins: Antimicrobial spectrum and complete inhibition of Listeria monocytogenes in a refrigerated food matrix. *CyTA–J. Food* 2019, 17, 228−239.

(26) Widiyastuti, Y.; Pratiwi, R.; Riyanto, S.; Wahyuono, S. Cytotoxic activity and apoptosis induction of avocado Persea americana Mill. seed extract on MCF-7 cancer cell line. *Indones. J. Biotechnol.* 2018, 23, 61−67.

(27) Dabas, D.; Shegog, R.; Ziegler, G.; Lambert, J. Avocado (Persea americana) seed as a source of bioactive phytochemicals. *Curr. Pharm. Des.* 2013, 19, 6133−6140.

(28) Chao, P.-Y.; Lin, S.-Y.; Lin, K.-H.; Liu, Y.-F.; Hsu, J.-I.; Yang, C.-M.; Lai, J.-Y. Antioxidant activity in extracts of 27 indigenous Taiwanese vegetables. *Nutrients* 2014, 6, 2115−2130.

(29) Mazza, G.; Fukumoto, L.; Delaquis, P.; Girard, B.; Ewert, B. Anthocyanins, phenolics, and color of Cabernet franc, Merlot, and Pinot noir wines from British Columbia. *J. Agric. Food Chem.* 1999, 47, 4009−4017.

(30) Alabi, T. D.; Brooks, N. L.; Oguntibeju, O. O. Antioxidant capacity, phytochemical analysis and identification of active compounds in anchomanes difformis. *Nat. Prod. J.* 2020, 10, 446−458.

(31) Waterhouse, A. *Folin-Ciocalteu Method for Total Phenol in Wine* [Online]; Department of Viticulture & Enology, University of California, Davis, 2005. Available from: http://waterhouse.ucdavis.edu/phenol/folinmicro (accessed October 5, 2011).

(32) Ou, B.; Huang, D.; Hampsch-Woodill, M.; Flanagan, J. A.; Deemer, E. K. Analysis of antioxidant activities of common vegetables employing oxygen radical absorbance capacity (ORAC) and ferric reducing antioxidant power (FRAP) assays: a comparative study. *J. Agric. Food Chem.* 2002, 50, 3122−3128.

(33) Lim, C. S. H.; Lim, S. L. Ferric reducing capacity versus ferric reducing antioxidant power for measuring total antioxidant capacity. *Lab. Med.* 2013, 44, 51−55.

(34) Benzie, I. F.; Strain, J. J. The ferric reducing ability of plasma (FRAP) as a measure of "antioxidant power": the FRAP assay. *Anal. Biochem.* 1996, 239, 70−76.

(35) Nordin, N.; Yeap, S. K.; Rahman, H. S.; Zamberi, N. R.; Abu, N.; Mohamad, N. E.; How, C. W.; Masarudin, M. J.; Abdullah, R.; Alitheen, N. B. In vitro cytotoxicity and anticancer effects of citral nanostructured lipid carrier on MDA MBA-231 human breast cancer cells. *Sci. Rep.* 2019, 9, 1614.

(36) Seo, Y. S.; Ahn, E.-Y.; Park, J.; Kim, T. Y.; Hong, J. E.; Kim, K.; Park, Y.; Park, Y. Catalytic reduction of 4-nitrophenol with gold nanoparticles synthesized by caffeic acid. *Nanoscale Res. Lett.* **2017**, *12*, 7.

(37) Oueslati, M. H.; Ben Tahar, L.; Harrath, A. H. Synthesis of ultra-small gold nanoparticles by polyphenol extracted from Salvia officinalis and efficiency for catalytic reduction of p-nitrophenol and methylene blue. *Green Chem. Lett. Rev.* **2020**, *13*, 18−26.

(38) Madiehe, A. M.; Moabelo, K. L.; Modise, K.; Sibuyi, N. R.; Meyer, S.; Dube, A.; Onani, M. O.; Meyer, M. Catalytic reduction of 4-nitrophenol and methylene blue by biogenic gold nanoparticles synthesized using Carpobrotus edulis fruit (sour fig) extract. *Nanomater. Nanotechnol.* **2022**, *12*, 18479804221108254.

(39) Zeiri, Y.; Elia, P.; Zach, R.; Hazan, S.; Kolusheva, S.; Porat, Z. Green synthesis of gold nanoparticles using plant extracts as reducing agents. *Int. J. Nanomed.* **2014**, *9*, 4007.

(40) Mulvaney, P. Surface plasmon spectroscopy of nanosized metal particles. *Langmuir* **1996**, *12*, 788−800.

(41) Al-Azad, S.; Morshed, M. N.; Deb, H.; Alam, M.; Hasan, K. F.; Shen, X. Localized Surface Plasmon Resonance Property of Ag-Nanoparticles and Prospects as Imminent Multi-Functional Colorant. *Am. J. Nanosci. Nanotechnol. Res.* **2017**, *5*, 1−20.

(42) Wadhwani, S. A.; Shedbalkar, U. U.; Singh, R.; Karve, M. S.; Chopade, B. A. Novel polyhedral gold nanoparticles: green synthesis, optimization and characterization by environmental isolate of Acinetobacter sp. SW30. *World J. Microbiol. Biotechnol.* **2014**, *30*, 2723−2731.

(43) Rajeshkumar, S.; Kumar, S. V.; Malarkodi, C.; Vanaja, M.; Paulkumar, K.; Annadurai, G. Optimized Synthesis of Gold Nanoparticles Using Green Chemical Process and Its Invitro Anticancer Activity Against HepG2 and A549 Cell Lines. *Mech., Mater. Sci. Eng. J.* **2017**, *9*. DOI: 10.2412/mmse.95.26.479

(44) Fazal, S.; Jayasree, A.; Sasidharan, S.; Koyakutty, M.; Nair, S. V.; Menon, D. Green synthesis of anisotropic gold nanoparticles for photothermal therapy of cancer. *ACS Appl. Mater. Interfaces* **2014**, *6*, 8080−8089.

(45) Latif, M. S.; Kormin, F.; Mustafa, M. K.; Mohamad, I. I.; Khan, M.; Abbas, S.; Ghazali, M. I.; Shafie, N. S.; Bakar, M. F. A.; Sabran, S. F. Effect of temperature on the synthesis of Centella asiatica flavonoids extract-mediated gold nanoparticles: UV-visible spectra analyses. In *AIP Conference Proceedings*; AIP Publishing LLC, 2018.

(46) Verma, A.; Mehata, M. S. Controllable synthesis of silver nanoparticles using Neem leaves and their antimicrobial activity. *J. Radiat. Res. Appl. Sci.* **2016**, *9*, 109−115.

(47) Basiratnia, E.; Einali, A.; Azizian-Shermeh, O.; Mollashahi, E.; Ghasemi, A. Biological Synthesis of Gold Nanoparticles from Suspensions of Green Microalga Dunaliella salina and Their Antibacterial Potential. *BioNanoScience* **2021**, *11*, 977−988.

(48) Desai, M. P.; Sangaokar, G. M.; Pawar, K. D. Kokum fruit mediated biogenic gold nanoparticles with photoluminescent, photo-catalytic and antioxidant activities. *Process Biochem.* **2018**, *70*, 188−197.

(49) Feng, Y.; Yu, Y.; Wang, Y.; Lin, X. Biosorption and bioreduction of trivalent aurum by photosynthetic bacteria Rhodobacter capsulatus. *Curr. Microbiol.* **2007**, *55*, 402−408.

(50) Unal, I. S.; Demirbas, A.; Onal, I.; Ildiz, N.; Ocsoy, I. One step preparation of stable gold nanoparticle using red cabbage extracts under UV light and its catalytic activity. *J. Photochem. Photobiol., B* **2020**, *204*, 111800.

(51) Ahmad, A.; Senapati, S.; Khan, M. I.; Kumar, R.; Sastry, M. Extracellular biosynthesis of monodisperse gold nanoparticles by a novel Extremophilic actinomycete, Thermomonospora sp. *Langmuir* **2003**, *19*, 3550−3553.

(52) Mishra, A.; Tripathy, S. K.; Yun, S.-I. Fungus mediated synthesis of gold nanoparticles and their conjugation with genomic DNA isolated from Escherichia coli and Staphylococcus aureus. *Process Biochem.* **2012**, *47*, 701−711.

(53) Torres-Chavolla, E.; Ranasinghe, R. J.; Alocilja, E. C. Characterization and functionalization of biogenic gold nanoparticles

(54) Bawazeer, S.; Khan, I.; Rauf, A.; Aljohani, A. S.; Alhumaydhi, F. A.; Khalil, A. A.; Qureshi, M. N.; Ahmad, L.; Khan, S. A. Black pepper (Piper nigrum) fruit-based gold nanoparticles (BP-AuNPs): Synthesis, characterization, biological activities, and catalytic applications−A green approach. *Green Process. Synth.* **2022**, *11*, 11−28.

(55) Chandran, K.; Song, S.; Yun, S.-I. Effect of size and shape controlled biogenic synthesis of gold nanoparticles and their mode of interactions against food borne bacterial pathogens. *Arabian J. Chem.* **2019**, *12*, 1994−2006.

(56) Dube, P.; Meyer, S.; Madiehe, A.; Meyer, M. Antibacterial activity of biogenic silver and gold nanoparticles synthesized from Salvia africana-lutea and Sutherlandia frutescens. *Nanotechnology* **2020**, *31*, 505607.

(57) Pandey, S.; Oza, G.; Mewada, A.; Sharon, M. Green synthesis of highly stable gold nanoparticles using Momordica charantia as nano fabricator. *Arch. Appl. Sci. Res.* **2012**, *4*, 1135−1141.

(58) Demirbas, A.; Büyükbezirci, K.; Celik, C.; Kislakci, E.; Karaagac, Z.; Gokturk, E.; Kati, A.; Cimen, B.; Yilmaz, V.; Ocsoy, I. Synthesis of long-term stable gold nanoparticles benefiting from red raspberry (Rubus idaeus), strawberry (Fragaria ananassa), and blackberry (Rubus fruticosus) extracts−gold ion complexation and investigation of reaction conditions. *ACS Omega* **2019**, *4*, 18637−18644.

(59) Hazarika, M.; Kalita, G. D.; Pramanik, S.; Borah, D.; Das, P. Bio-functionalized anisotropic gold nanoparticles as efficient catalyst for nitrile hydration and hydrogenation of nitrophenol. *Curr. Res. Green Sustainable Chem.* **2020**, *3*, 100018.

(60) Kathuria, D.; Bhattu, M.; Sharma, A.; Sareen, S.; Verma, M.; Kumar, S. Catalytic Reduction of Water Contaminants Using Green Gold Nanoparticles Mediated by Stem Extract of Nepeta Leucophylla. *Top. Catal.* **2022**, *65*, 1899−1909.

(61) Samsulkahar, N. F.; Hadi, A. A.; Shamsuddin, M.; Nik, N. A. N. Biosynthesis of Gold Nanoparticles Using Strobilanthes crispa Aqueous Leaves Extract and Evaluation of Its Antibacterial Activity. *Biointerface Res. Appl. Chem.* **2023**, *13*, 63.

(62) Geraldes, A. N.; da Silva, A. A.; Leal, J.; Estrada-Villegas, G. M.; Lincopan, N.; Katti, K. V.; Lug&atildeo, A. B. Green nanotechnology from plant extracts: synthesis and characterization of gold nano-particles. *Adv. Nanopart.* **2016**, *05*, 176−185.

(63) Elbagory, A. M.; Cupido, C. N.; Meyer, M.; Hussein, A. A. Large scale screening of Southern African plant extracts for the green synthesis of gold nanoparticles using microtitre-plate method. *Molecules* **2016**, *21*, 1498.

(64) Mmola, M.; Roes-Hill, M. L.; Durrell, K.; Bolton, J. J.; Sibuyi, N.; Meyer, M. E.; Beukes, D. R.; Antunes, E. Enhanced antimicrobial and anticancer activity of silver and gold nanoparticles synthesised using Sargassum incisifolium aqueous extracts. *Molecules* **2016**, *21*, 1633.

(65) Bogireddy, N.; Pal, U.; Gomez, L. M.; Agarwal, V. Size controlled green synthesis of gold nanoparticles using Coffea arabica seed extract and their catalytic performance in 4-nitrophenol reduction. *RSC Adv.* **2018**, *8*, 24819−24826.

(66) Yin, X.; Chen, S.; Wu, A. Green chemistry synthesis of gold nanoparticles using lactic acid as a reducing agent. *Micro Nano Lett.* **2010**, *5*, 270−273.

(67) Joy Prabu, H.; Johnson, I. Plant-mediated biosynthesis and characterization of silver nanoparticles by leaf extracts of Tragia involucrata, Cymbopogon citronella, Solanum verbascifolium and Tylophora ovata. *Karbala Int. J. Mod. Sci.* **2015**, *1*, 237−246.

(68) Chen, Z.; Paley, D. W.; Wei, L.; Weisman, A. L.; Friesner, R. A.; Nuckolls, C.; Min, W. Multicolor live-cell chemical imaging by isotopically edited alkyne vibrational palette. *J. Am. Chem. Soc.* **2014**, *136*, 8027−8033.

(69) Kaur, A.; Preet, S.; Kumar, V.; Kumar, R.; Kumar, R. Synergetic effect of vancomycin loaded silver nanoparticles for enhanced antibacterial activity. *Colloids Surf., B* **2019**, *176*, 62−69.

for biosensing enhancement. *IEEE Trans. Nanotechnol.* **2010**, *9*, 533−538.

(70) Sanghi, R.; Verma, P. pH dependant fungal proteins in the 'green'synthesis of gold nanoparticles. *Adv. Mater. Lett.* **2010**, *1*, 193–199.

(71) Fregue, T. T. R.; Ionel, I.; Gabche, A. S.; Mihaiuti, A.-C. Optimization of the activated carbon preparation from avocado seeds, using the response surface methodology. *Rev. Chim.* **2019**, *70*, 410–416.

(72) Ajitha, B.; Ashok Kumar Reddy, Y.; Sreedhara Reddy, P. Green synthesis and characterization of silver nanoparticles using Lantana camara leaf extract. *Mater. Sci. Eng., C* **2015**, *49*, 373–381.

(73) Dorosti, N.; Jamshidi, F. Plant-mediated gold nanoparticles by Dracocephalum kotschyi as anticholinesterase agent: Synthesis, characterization, and evaluation of anticancer and antibacterial activity. *J. Appl. Biomed.* **2016**, *14*, 235–245.

(74) Balashanmugam, P.; Durai, P.; Balakumaran, M. D.; Kalaichelvan, P. T. Phytosynthesized gold nanoparticles from C. roxburghii DC. leaf and their toxic effects on normal and cancer cell lines. *J. Photochem. Photobiol., B* **2016**, *165*, 163–173.

(75) Bogireddy, N. K. R.; Agarwal, V. Persea americana seed extract mediated gold nanoparticles for mercury (ii)/iron (iii) sensing, 4-nitrophenol reduction, and organic dye degradation. *RSC Adv.* **2019**, *9*, 39834–39842.

(76) Setyawan, H.; Sukardi, S.; Puriwangi, C. Phytochemicals properties of avocado seed: A review. In *IOP Conference Series: Earth and Environmental Science*; IOP Publishing, 2021.

(77) Mohanta, Y. K.; Panda, S. K.; Biswas, K.; Tamang, A.; Bandyopadhyay, J.; De, D.; Mohanta, D.; Bastia, A. K. Biogenic synthesis of silver nanoparticles from Cassia fistula (Linn.): In vitro assessment of their antioxidant, antimicrobial and cytotoxic activities. *IET Nanobiotechnol.* **2016**, *10*, 438–444.

(78) Vo, T. S.; Ngo, D.; Le, P. Free radical scavenging and anti-proliferative activities of avocado (Persea americana Mill.) seed extract. *Asian Pac. J. Trop. Biomed.* **2019**, *9*, 91.

(79) Dabas, D.; Elias, R. J.; Ziegler, G. R.; Lambert, J. D. In vitro antioxidant and cancer inhibitory activity of a colored avocado seed extract. *Int. J. Food Sci.* **2019**, *2019*, 6509421.

(80) Bangar, S. P.; Dunno, K.; Dhull, S. B.; Kumar Siroha, A.; Changan, S.; Maqsood, S.; Rusu, A. V. Avocado seed discoveries: Chemical composition, biological properties, and industrial food applications. *Food Chem.: X* **2022**, *16*, 100507.

(81) Li, M.; Chen, G. Revisiting catalytic model reaction p-nitrophenol/NaBH 4 using metallic nanoparticles coated on polymeric spheres. *Nanoscale* **2013**, *5*, 11919–11927.

(82) Chiou, J.-R.; Lai, B.-H.; Hsu, K.-C.; Chen, D.-H. One-pot green synthesis of silver/iron oxide composite nanoparticles for 4-nitrophenol reduction. *J. Hazard. Mater.* **2013**, *248–249*, 394–400.

(83) Das, T. K.; Das, N. C. Advances on catalytic reduction of 4-nitrophenol by nanostructured materials as benchmark reaction. *Int. Nano Lett.* **2022**, *12*, 223–242.

(84) Iben Ayad, A.; Luart, D.; Ould Dris, A.; Guénin, E. Kinetic analysis of 4-nitrophenol reduction by "water-soluble" palladium nanoparticles. *Nanomaterials* **2020**, *10*, 1169.

(85) Lin, F.-h.; Doong, R.-a. Highly efficient reduction of 4-nitrophenol by heterostructured gold-magnetite nanocatalysts. *Appl. Catal., A* **2014**, *486*, 32–41.

(86) Seo, Y. S.; Ahn, E.-Y.; Park, J.; Kim, T. Y.; Hong, J. E.; Kim, K.; Park, Y.; Park, Y. Catalytic reduction of 4-nitrophenol with gold nanoparticles synthesized by caffeic acid. *Nanoscale Res. Lett.* **2017**, *12*, 7.

(87) Islam, M. T.; Jing, H.; Yang, T.; Zubia, E.; Goos, A. G.; Bernal, R. A.; Botez, C. E.; Narayan, M.; Chan, C. K.; Noveron, J. C. Fullerene stabilized gold nanoparticles supported on titanium dioxide for enhanced photocatalytic degradation of methyl orange and catalytic reduction of 4-nitrophenol. *J. Environ. Chem. Eng.* **2018**, *6*, 3827–3836.

(88) Gangula, A.; Podila, R.; Karanam, L.; Karanam, L.; Janardhana, C.; Rao, A. M. Catalytic reduction of 4-nitrophenol using biogenic gold and silver nanoparticles derived from Breynia rhamnoides. *Langmuir* **2011**, *27*, 15268–15274.

(89) Neal, R. D.; Inoue, Y.; Hughes, R. A.; Neretina, S. Catalytic reduction of 4-nitrophenol by gold catalysts: the influence of borohydride concentration on the induction time. *J. Phys. Chem. C* **2019**, *123*, 12894–12901.

(90) Trivedi, M. U.; Patlolla, C. K.; Misra, N. M.; Pandey, M. K. Cucurbit [6] uril glued magnetic clay hybrid as a catalyst for nitrophenol reduction. *Catal. Lett.* **2019**, *149*, 2355–2367.

(91) Liang, M.; Su, R.; Huang, R.; Qi, W.; Yu, Y.; Wang, L.; He, Z. Facile in situ synthesis of silver nanoparticles on procyanidin-grafted eggshell membrane and their catalytic properties. *ACS Appl. Mater. Interfaces* **2014**, *6*, 4638–4649.

(92) Lomonosov, V.; Asselin, J.; Ringe, E. Solvent effects on the kinetics of 4-nitrophenol reduction by NaBH 4 in the presence of Ag and Au nanoparticles. *React. Chem. Eng.* **2022**, *7*, 1728–1741.